

1 **Intermittent upwelling events trigger delayed, major,**
2 **and reproducible pico-nanophytoplankton responses in**
3 **coastal oligotrophic waters**

4 **R. Fuchs^{1,2*}, V. Rossi^{2†}, C. Caille^{3‡},**
5 **N. Bensoussan^{2§}, C. Pinazo^{2¶}, O. Grosso^{2||}, M. Thyssen^{2**}**

6 ¹Aix Marseille Univ, CNRS, Centrale Marseille, I2M, Marseille, France
7 ²Aix Marseille Univ, Université de Toulon, CNRS, IRD, MIO, Marseille, France
8 ³Sorbonne Université, CNRS, LOMIC, Banyuls-sur-Mer, France

9 **Key Points:**

- 10 • Phytoplankton abundance (biomass, resp.) reactions start less than 2 days (4 days,
11 resp.) after the upwelling onset and last 2 to 5 days.
12 • Except for *Synechococcus*, all group biomasses increase by 50-173% (up to +400%)
13 during each event, then sharply decrease back to normal.
14 • Biomass peaks and daily rates of increase induced by the most extreme upwellings
15 are of the same magnitude as the spring bloom ones.

*robin.fuchs@univ-amu.fr

†vincent.rossi@mio.osupytheas.fr

‡caillec@obs-banyuls.fr

§nathaniel.bensoussan@mio.osupytheas.fr

¶christel.pinazo@mio.osupytheas.fr

||olivier.grosso@mio.osupytheas.fr

**melilotus.thyssen@mio.osupytheas.fr

Corresponding author: Melilotus Thyssen, melilotus.thyssen@mio.osupytheas.fr

Abstract

Pico-nanophytoplankton organisms are dominant in oligotrophic areas of the ocean thanks to competitive skills in nutrient-depleted waters. Their small cell size and highly adaptive growth rates make their contribution to the oceanic carbon cycle difficult to estimate. Despite the recent recognition of rapid and marked environmental shifts impact on microbial communities, the response capacities of pico-nanophytoplankton remain poorly studied. Here we address this knowledge gap in a coastal Mediterranean station influenced by intermittent wind gusts causing sporadic upwelling events. Within a few days after the wind rises, upwellings result in short-lived nutrient pulses and seawater temperature drops of up to 10°C lasting six days on average. Using a CytoSense flow cytometer continuously operating at a two-hour frequency from September 2019 to November 2021, we monitored the abundances and biomass of five phytoplankton functional groups over two complete annual cycles. Using unsupervised signal rupture-detection methods, our investigations focus on events forced by north-westerlies when the water column is stratified in late spring, summer, and early fall, corresponding to oligotrophic conditions. We show that despite their short durations, these events repeatedly trigger delayed increases in both abundances and biomasses for most pico-nanophytoplankton groups that can overpass spring bloom values. These positive biological reactions last two to five days and are immediately followed by an overall drop evidencing a clear physical driver of the biomass peaks. Not considering these submesoscale events, which are currently not reproduced by climate models, and the fast and salient biological responses they trigger may significantly bias carbon budgets.

Plain Language Summary

Short-lived north-westerlies in the Mediterranean sea replace surface coastal waters with colder and richer in nutrients deeper waters from offshore. This phenomenon, called a sporadic upwelling event, lasts only a few days after the wind stops and induces brutal environmental shifts. During summer, upwellings generate drops in surface water temperature of up to 10°C and are expected to have a significant impact on phytoplankton cells. Small phytoplankton cells are conspicuous for their fast response to environmental changes thanks to their high division rates (up to several times a day). As a result, the biological response to wind-induced upwellings has to be studied using high-frequency measurements. Using four attributes for each of the five studied phytoplankton groups, we show that the number of cells of most groups rose strongly in less than two days after the temperature drop according to remarkable repeatable patterns. Similarly, their carbon content increased after less than four days. The reactions themselves lasted up to five days before going back near to the initial level. The described phytoplankton reactions to local upwelling events can be as important as the ones observed during the spring bloom, often regarded as the most important seasonal event for phytoplankton communities.

1 Introduction

Coastal zones play a significant role in the global carbon cycle as they sustain, despite large uncertainties, up to 30% of the global oceanic primary production (Gattuso et al., 1998). Previous research suggested the importance of taking into account the diversity and variability of near-shore ecosystems, which remain poorly known and under the influences of complex physical forcing (Borges et al., 2005; Bauer et al., 2013; Wimart-Rousseau et al., 2020) that strongly shapes phytoplankton communities (Morel & André, 1991; Antoine et al., 1995; Bosc et al., 2004; Armbrrecht et al., 2014). Furthermore, there is evidence of the fast response capacities of phytoplankton after environmental changes, notably considering the prominence of meso and submesoscale processes in the ocean (Lévy et al., 2012). This is especially true for the pico-nanophytoplankton cells that present

66 adaptive growth rates enhancing their competitive strategies (Lomas et al., 2009). The
67 pico-nanophytoplankton size class is composed of polyphyletic unicellular photosynthetic
68 microorganisms that dominate primary production in oligotrophic basins (Li, 1995; Grob
69 et al., 2007) and are dominant in less oligotrophic conditions outside of the main spring
70 and autumn bloom periods (Bolaños et al., 2020). They contribute substantially to the
71 export of organic carbon into the deep layers mainly by aggregation or via grazing and
72 subsequent sinking of organic materials (Richardson & Jackson, 2007; Lomas & Moran,
73 2011).

74 To assess the typical speed and frequency of community shifts that inform the ca-
75 pacity of pico-nanophytoplankton adaptation to abrupt changes in their environment,
76 long-term and high-frequency sampling strategies allowing the separation of phytoplank-
77 ton cells into functionally meaningful size classes are required. Martin-Platero et al. (2018)
78 relied on a time series composed of daily samples for 93 days to show that physical forc-
79 ing strongly shapes phytoplankton communities and that the observed patterns were highly
80 dependent on the sampling frequency. Similarly, Martiny et al. (2016) have demonstrated
81 positive significant correlations of cyanobacteria, pico and nanoeukaryotes abundances
82 with temperature as well as nutrients using weekly samples over three years. Hunter-Cevera
83 et al. (2020) used a 16-year long time series at an hourly frequency to highlight the sea-
84 sonal cycles of *Synechococcus* abundances and proposed an explanation for *Synechococ-*
85 *cus* blooms relying on growth rates variations. Wilkerson et al. (2006) demonstrated that
86 wind-induced upwelling events followed by relaxation periods trigger optimal growth con-
87 ditions for phytoplankton cells, depleting the upwelled nutrients and fostering a commu-
88 nity of large phytoplanktonic cells (e.g. large diatoms), in line with Rossi et al. (2013).
89 In more oligotrophic coastal areas, the responses of phytoplanktonic communities to short-
90 lived enrichment events are more puzzling (Armbrecht et al., 2014) and suggest the promi-
91 nence of small-sized phytoplanktonic cells. Thyssen et al. (2008) and Dugenne et al. (2014)
92 have indeed shown important responses of pico-nanophytoplankton groups after strong
93 north-westerlies events in the Bay of Marseille. Apart from atmospheric or riverine in-
94 puts and other classes of submesoscale frontal dynamics, sporadic wind-driven upwelling
95 events are one major source of nutrients in the surface layers of various oligotrophic coastal
96 areas (Millot, 1979; Bakun & Agostini, 2001; Palma & Matano, 2009; Rossi et al., 2014).
97 While their hydrographic impacts, temperature cooling and nutrient enrichment of sur-
98 face waters, are relatively well documented, little information exists on how they influ-
99 ence phytoplankton communities. The Bay of Marseille constitutes a natural laboratory
100 to study the biological impacts of such events since they are common during stratified
101 summer periods (Odic et al., 2022).

102 To our knowledge, all previous studies did not focus on wind events exclusively (Martiny
103 et al., 2016; Hunter-Cevera et al., 2020), had low statistical power (Thyssen et al., 2008;
104 Dugenne et al., 2014; Martin-Platero et al., 2018), had an insufficient temporal resolu-
105 tion (daily frequency for Wilkerson et al. (2006), weekly frequency in Martiny et al. (2016))
106 or did not fully resolve the pico-nanophytoplankton size class (Wilkerson et al., 2006;
107 García-Reyes et al., 2014; Hunter-Cevera et al., 2020). In this study, we analyzed twenty
108 short-lived wind-driven events occurring when the water column was stratified (late spring,
109 summer, and early fall) allowing the detection of clear upwelling signatures in compar-
110 ison to unstratified periods. The causal effect of the physical forcing was identified us-
111 ing a bi-hourly time series capturing the dynamics of five phytoplankton functional groups
112 as resolved by Automated Flow Cytometry (Dubelaar & Gerritzen, 2000; Olson et al.,
113 2003) over two complete years. The area of interest is the French Bay of Marseille, which
114 is considered oligotrophic in stratified periods during which it is generally affected by
115 the regional offshore bloom occurring in winter-early spring and fall seasons (d’Ortenzio
116 & Ribera d’Alcalà, 2009). It is dominated by pico-nanophytoplankton size classes and
117 its hydrology is strongly influenced by North-westerlies winds generating regularly short-
118 lived upwelling events (Bensoussan et al., 2010; Pairaud et al., 2011; Fraysse et al., 2013;
119 Lajaunie-Salla et al., 2021; Odic et al., 2022).

2 Materials and Methods

The temperature, nutrients, and phytoplankton data were collected from September 19, 2019, to November 31, 2021, at the Sea Water Sensing Laboratory @ MIO Marseille (SSL@MM), a coastal marine station in the North-West Mediterranean Sea (43°17' N, 5°22' E). Seawater was continuously pumped at 10 meters from the coastline at a depth of 3 meters and delivered into the laboratory using a VerderFlex 40 peristaltic pump. The seawater was coarsely pre-filtered by a PVC strainer (3 mm) and routed by polypropylene pipes that are cleaned monthly.

The temperature data were acquired every hour using an STPS sensor from the NKE-manufacturer presenting a temperature accuracy of 0.05°C. Nutrient samples were collected every four days on average and stored at -20°C until they were analyzed in a laboratory using a Technicon Autoanalyser® (SEAL Analytical) as in Tréguer and Le Corre (1975).

2.1 Phytoplankton Acquisition by Automated Pulse-shape Recording Flow Cytometry

Phytoplankton data were sampled every two hours using an Automated pulse-shape recording Flow Cytometer (Dubelaar et al., 1999; Dubelaar & Gerritzen, 2000) with the same protocol as in Marrec et al. (2018). We relied on the nomenclature proposed by Thyssen et al. (2021) (<http://vocab.nerc.ac.uk/collection/F02/current/>) and resolved five phytoplankton functional groups (PFGs): Redpicopro, Orgpicopro, Redpicoeuk, Rednano, and Orgnano, which were previously often referred to as *Prochlorococcus*, *Synechococcus*, picoeukaryotes, nanoeukaryotes, and cryptophytes, respectively. Microphytoplankton cells were collected but were not representative enough to be reported here: 75% of the samples presented less than 13 particles per milliliter. Each cell was assigned to a PFG by a Convolutional Neural Network (CNN) introduced in Fuchs et al. (2022).

2.2 Phytoplankton Biovolume, Biomass, and Growth Rate Estimations

Biovolume and biomass were estimated through empirical relationships (see Figure S1, sections 1.2 and 1.3 in Supplemental Information) following Marrec et al. (2018). The functional groups growth rate was estimated from the cell biovolumes using a size-structured population model introduced by Sosik et al. (2003) and adapted by Ribalet et al. (2015).

2.3 Wind-driven Upwelling Signatures

The occurrence and strength of each upwelling event were assessed based on the positive values of the Wind-driven Upwelling/Downwelling Index (WUDI) developed and extensively validated by Odic et al. (2022). The drop in temperature generated during an upwelling-favorable wind was evaluated as the difference between the measured water temperature and its low-pass filtered time series using a cut-off frequency of 15 days as in Rossi et al. (2014) and Odic et al. (2022). These temperature drops, or anomalies, were used to delimit three physical phases (Figure 2): (i) a pre-anomaly phase when the water temperature is stable and high, (ii) an anomaly phase when the temperature drops, stays cool for a few hours/days to then warm-up slowly, and (iii) a post-anomaly phase when the temperature has returned to a warmer and more stable state. These anomalies are particularly significant during the summer when the water column is stratified. A period was considered stratified when the filtered temperature was higher than the annual average temperature and conversely for unstratified periods as in Odic et al. (2022). Among the 54 events recorded over two years, only 20 events occurred during stratified periods and had temperature and flow cytometry data available. Besides, all successive events marked with negative seawater temperature anomalies separated by less than one

169 day were not considered in order to have for each event a minimal relaxation time. In
 170 other words, we retain here only the significant wind-driven events happening in strat-
 171 ified periods that are surrounded by relatively calm periods, denoted "Stratified period
 172 Wind-induced Upwelling Event", SWUE.

173 The spring blooms occurring in unstratified periods were used to benchmark the
 174 biomass (and abundance) increases generated by SWUEs as the spring blooms are ex-
 175 pected to be the most productive periods (Frayse et al., 2013). The bloom dates were
 176 determined using the threshold method (Sapiano et al., 2012; Brody et al., 2013) and
 177 the median biomass and abundance per PFG during the bloom were used as the refer-
 178 ence benchmark level. The biomass increase imputable to the blooms was computed us-
 179 ing the median biomass during the week preceding the bloom as a reference value.

180 2.4 Rupture Detection and Response Characterization

181 The biological response of each PFG to the SWUE was evaluated in terms of both
 182 abundances and biomasses using a statistically-based rupture detection method presented
 183 in Truong et al. (2020). This mathematically well-founded method looked for ruptures
 184 in causal time series. It is here employed to detect potential changes in the link exist-
 185 ing between the temperature signal and each PFG abundance or biomass. The link was
 186 here assumed to be linear (Bai & Perron, 2003) and rupture detections were performed
 187 on biomasses and abundances separately. This methodology encompasses the idea that
 188 PFGs respond to a change in their environment, and delimited the start and end of the
 189 reactions for each PFG. The response of each PFG is hence composed of three phases:
 190 a pre-reaction, a reaction, and a post-reaction phase (called the relaxation phase).

191 Based on the identified ruptures, four key variables per PFG were used to charac-
 192 terize the duration and magnitude of the biological responses as presented in Figure 2
 193 a). The reaction delay is the time taken by a PFG to react after the rise of physical forc-
 194 ing, i.e. between the start of the water cooling and the beginning of the PFG automat-
 195 ically identified reaction. The reaction duration measures the length of the reaction phase.
 196 The reaction and relaxation magnitudes are computed as the difference in medians dur-
 197 ing the pre-reaction and reaction phases and during the reaction and relaxation phases,
 198 respectively. To capture only PFGs causal responses to sporadic upwelling events, only
 199 the PFG responses for which the reactions occurred after the beginning of the anomaly
 200 phase were considered, which was the case for most events and PFGs. The number of
 201 SWUEs taken into account for each PFG is given in Figure 3.

202 More material and method details are given in Supplemental Information (section 1 and
 203 Figure S2).

204 3 Results

205 3.1 Seawater Temperature and Nutrients as Markers of Sporadic Up- 206 welling Events

207 The annual mean temperature over the three years was 17.8°C in 2019, 17.1°C in
 208 2020, and 17.3°C in 2021. The associated stratified periods started on May, 8 in 2020,
 209 and May, 25 in 2021 (not available in 2019), and ended on November, 13 in 2019, Oc-
 210 tober, 27 in 2020, and October, 31 in 2021. The number of significant and distinct SWUEs
 211 during the stratified periods was two in 2019, ten in 2020, and eight in 2021. The me-
 212 dian duration anomaly phase of the SWUEs was of six days and the subsequent drops
 213 in water temperature (difference between both maximal and minimal values recorded dur-
 214 ing each SWUE) varied from 0.7°C to 9.9°C, with a median value of 4.7°C (see also Odic
 215 et al. (2022)).

216 Nutrient concentrations and N/P ratio were higher during unstratified periods as
 217 compared to stratified periods, except for phosphate concentration (Figure S3 in Sup-
 218 plemental Information; Kruskal-Wallis test, p -value $\leq 1.0E-7$ for nitrites, nitrates, and
 219 N/P ratio, p -value ≤ 0.05 for ammonium). In stratified periods, the nitrite concentra-
 220 tion and N/P ratios were higher and nitrate concentration lower during SWUEs than
 221 outside the SWUEs. The concentrations of phosphate and ammonium were however com-
 222 parable during and outside the SWUEs. The N/P ratio was 25.15 in the unstratified pe-
 223 riod, 17.33 during SWUEs, and 13.05 in the stratified period outside of the SWUEs. Yet,
 224 only the nitrite concentrations recorded during and outside SWUEs under stratified con-
 225 ditions were significantly different (Kruskal-Wallis test, p -value = 0.034). The concen-
 226 trations are given in Table S1 in Supplemental Information.

227 3.2 Wind-induced Upwelling Events Trigger Peaks of Biomass and Abun- 228 dances

229 All SWUEs triggered noticeable peaks of biomass for most PFGs (Figure 1 and Fig-
 230 ure S4 in Supplemental Information). The pico-nanophytoplankton biomass was domi-
 231 nated in both stratification regimes by Rednano cells, followed by Orgnano, Orgpicopro,
 232 Redpicoeuk, and Redpicopro cells (Table S2 in Supplemental Information). Orgnano
 233 exceeded their median bloom biomass during one-third of the SWUEs. Similarly, more
 234 than half of the Orgpicopro and Rednano peaks went over their median bloom values.
 235 Finally, Redpicoeuk and Redpicopro biomass peak values were higher than their median
 236 bloom values in 4/5 SWUEs and all SWUEs, respectively.

237 In terms of abundance, the SWUEs generated peaks for most PFGs (Figure S5 in
 238 Supplemental Material). Over the whole series, the most abundant PFGs were the Org-
 239 picopro, followed by the Redpicopro, Redpicoeuk, Rednano, and Orgnano cells (Table
 240 S3 in Supplemental Information). Near the half of Orgnano and Orgpicopro SWUE abun-
 241 dance peaks exceeded their median bloom abundances. Besides, more than 4/5 of SWUEs
 242 saw Rednano, Redpicoeuk and Redpicopro abundances go higher than their respective
 243 median abundances during the spring bloom.

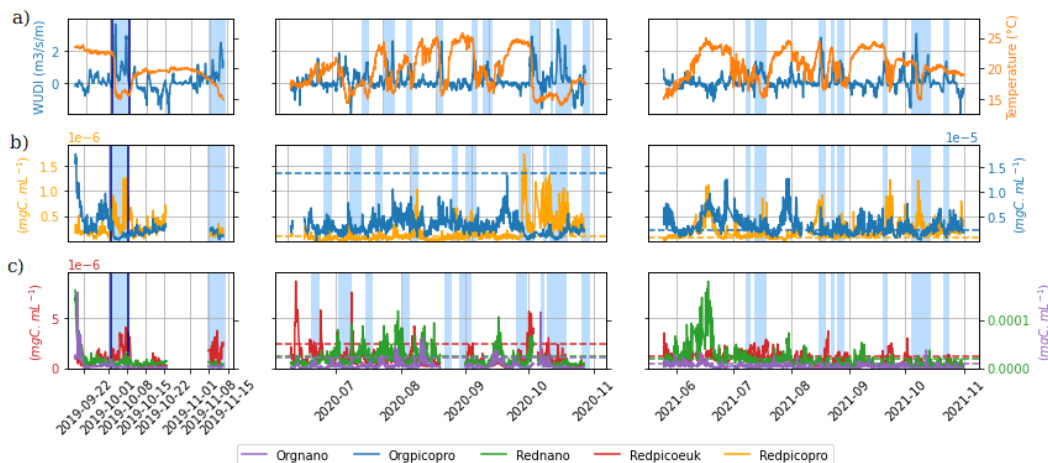


Figure 1. Time series of (a) Wind-driven Upwelling/Downwelling Index (WUDI, $m^3 \cdot s^{-1} \cdot m^{-1}$) and temperature ($^{\circ}C$) as well as (b, c) phytoplankton biomasses ($\mu gC \cdot mL^{-1}$) monitored at the SSL@MM coastal station. The blue rectangles correspond to the 20 studied SWUEs. The event shown in Figure 2 is bounded by a dark blue box. The horizontal dashed colored lines correspond to the median biomasses observed during the spring bloom (except for 2019, not available) for each PFG (according to the color code).

244 **3.3 Characterization of the Phytoplankton Response: A Single Event** 245 **Illustration**

246 The typical effect of wind-induced upwellings on temperature and pico-nanophytoplankton
247 biomass is illustrated in Figure 2, showing differentiated responses among the PFGs. This
248 event was fueled by three periods of intense wind forcings, or intensification periods, that
249 generated an abrupt drop in temperature (-7.6°C) followed by the maintenance of cold
250 waters for six days. As shown in Figure S6 in Supplemental Information, during these
251 three sub-events, the N/P ratio rose after each wind intensification with a short delay,
252 especially after the third one that multiplied the nitrates, nitrites, and phosphates con-
253 centration by a factor of 19, 5, and 5, respectively.

254 The biomass reactions of the Redpicopro, Orgpicopro, and Orgnano groups to this
255 SWUE were quasi-instantaneous while they appeared after a short delay for the Red-
256 picoeuk and Rednano cells (~ 3 days). The biomass reaction magnitude was $+42.7\%$ for
257 the Rednano, $+123.7\%$ for the Orgnano, $+178.7\%$ for the Redpicoeuk, $+377.3\%$ for the
258 Redpicopro, and -82.1% for the Orgpicopro. Biomass levels decreased in the relaxation
259 phase for all PFGs except the Orgnano.
260 The estimated hourly growth rates (Figure S7 in Supplemental Information) varied in-
261 versely with respect to the biomass (Figure 2) and the abundance (data not shown): when
262 the PFG was high in biomass, its growth rate was estimated to be low and conversely.

263 **3.4 Detailed Characterization of the Phytoplankton Response**

264 The PFG abundances showed reaction delays ranging between 24h and 36h in me-
265 dian (Figure 3a). The reaction duration of the PFGs lasted between three and four days
266 in median, with a lower Inter-Quartile Range (IQR)/median ratio than the reaction de-
267 lay (Figure 3e). Concerning the reaction magnitude, the Orgnano and Orgpicopro abun-
268 dances decreased while the other PFGs generally saw their abundances rising (Figure
269 3c). The Redpicopro and Redpicoeuk presented the largest increases in abundance. Their
270 large IQRs were explained by some intense positive reactions for the majority of the SWUEs
271 while only five presented moderately negative reactions for both groups. The abundance
272 levels in the relaxation period decreased for all PFGs with median variations ranging from
273 -28.96% to -52.85% (Figure 3g).

274 In terms of biomass, the Orgpicopro reacted in less than one day, the Orgnano and
275 Redpicopro in less than two days, and Rednano and Redpicoeuk median reaction delay
276 was three days (Figure 3b). The majority of reaction durations lasted between two and
277 five days (Figure 3f). The signs of the reactions remained the same as for the abundance,
278 except for the Orgnano that experienced a positive biomass reaction (Figure 3d). In the
279 relaxation periods, the biomass levels decreased for all PFGs (-27.58% to -61.90% in me-
280 dian). However, positive relaxation magnitudes were observed in five SWUEs both for
281 Orgpicopro and Rednano, explaining higher variance than for other PFGs (Figure 3h).

282 The estimated growth rates of the PFGs tended to slow down during the reaction
283 phase and then increase during the relaxation phase (Figure S8 in Supplemental Infor-
284 mation), except for the Orgpicopro. This pattern was however significant for Redpicoeuk
285 cells only (Kruskal-Wallis test, $p\text{-value} \leq 0.01$).

286 **4 Discussion**

287 The Bay of Marseille located in the NW Mediterranean upwelling system is a nat-
288 ural laboratory to explore the impact of wind-driven coastal processes on oligotrophic
289 communities because of the unique intensities and short duration of upwelling events (Odic
290 et al., 2022). During the stratified periods, the SWUEs had a clear signature on the sea-
291 water surface temperature. The expected signature on nutrient enrichment was less sig-

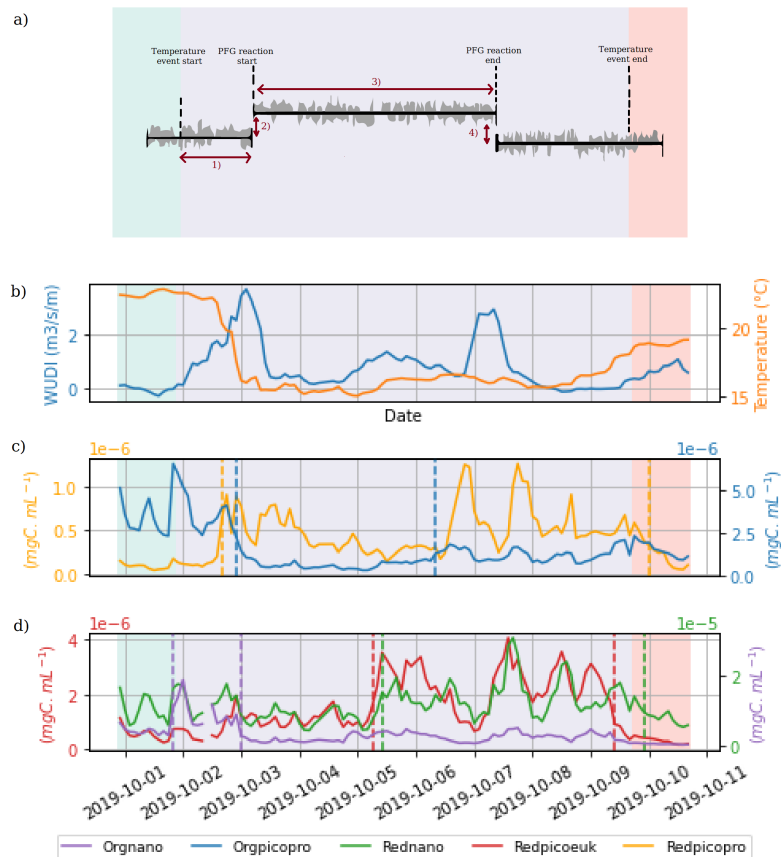


Figure 2. Illustrative view of a typical SWUE (highlighted by a dark blue box in Figure 1). a) Characterisation of the biological response to an SWUE. The grey-shaded time series represents a schematic PFG time series and the background shading corresponds to the temperature anomaly phases defining the physical event: pre-anomaly (green), anomaly (violet), and post-anomaly phase (red). The characterization is performed using four attributes: (1) the reaction delay, (2) the reaction magnitude, (3) the reaction duration, (4) and the relaxation magnitude. b) Variation of the WUDI ($m^3 \cdot s^{-1} \cdot m^{-1}$, blue line) and the temperature ($^{\circ}C$, orange line), c) Biomass ($mgC \cdot mL^{-1}$) of Redpicopro and Orgpicopro d) Biomass ($mgC \cdot mL^{-1}$) of Redpicoeuk, Rednano, and Orgnano. The vertical dashed lines represent the ruptures automatically detected by the statistical method for each PFG, according to the color code.

292 nificant, probably due to the littoral conditions, the delay needed for upwelled nutrients
 293 to reach the surface sampling point, but also largely to the low and irregular nutrient
 294 sampling rates (see Figure S3 in Supplemental Information).

295 As mentioned in García-Reyes et al. (2014), Rossi et al. (2014), and Armbrrecht et
 296 al. (2014), the physically-driven temperature drops and nutrient enrichments are key in-
 297 dicators to characterize the impact of SWUEs over the phytoplankton community. Us-
 298 ing a statistical rupture detection method, the causal effects of the environmental shifts
 299 over the pico-nanophytoplankton functional groups were assessed, capturing more than
 300 simple correlations and evidencing differentiated response patterns.

301 The phytoplankton functional groups reacted to the SWUEs in one to five days,
 302 a delay consistent with several studies evidencing phytoplankton biomass peaks two to

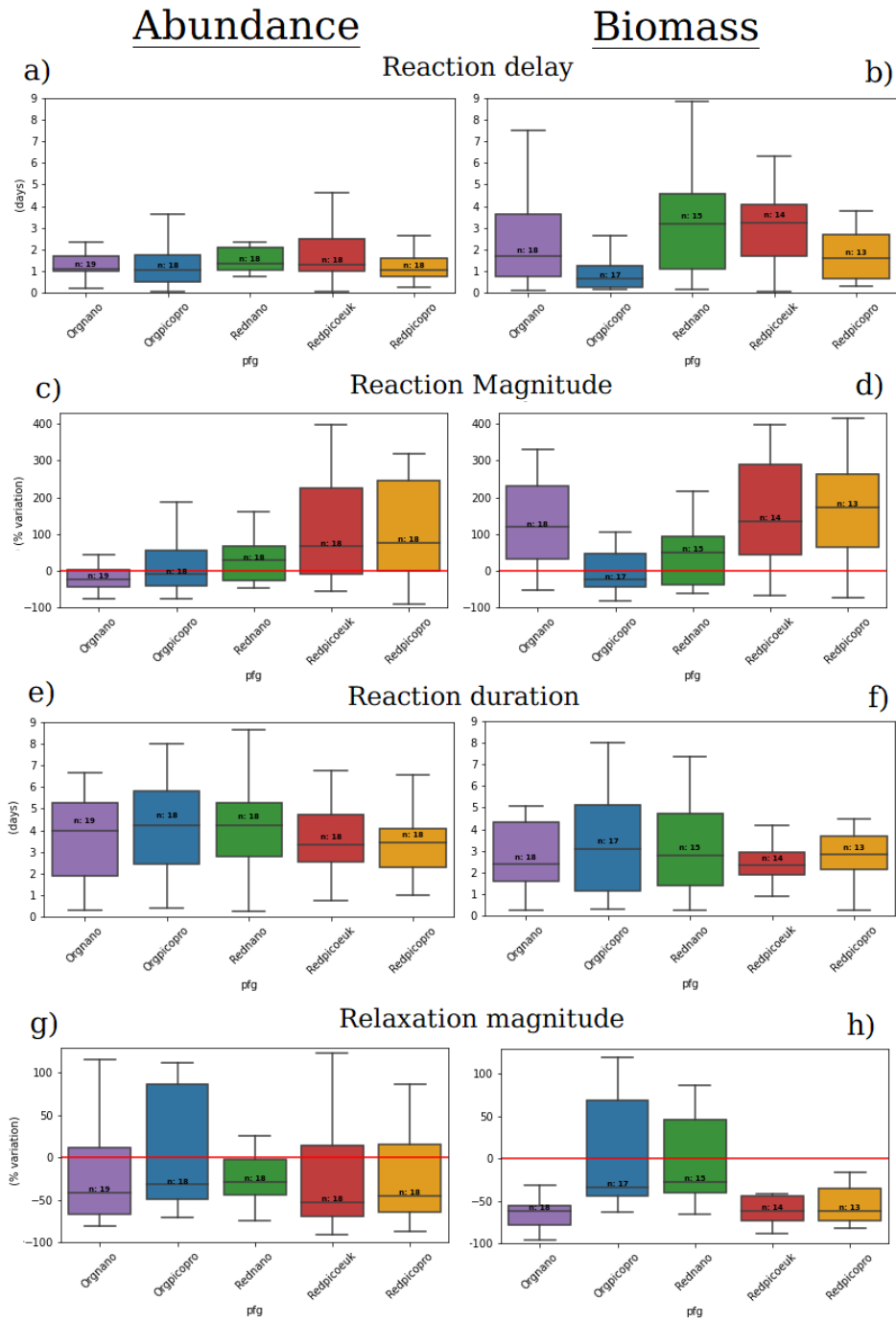


Figure 3. Boxplots of the reaction delay (a and b), the reaction magnitude (c and d), the reaction duration (e and f) and the relaxation magnitude (g and h) in terms of abundance and biomass, respectively, for five different PFGs. The horizontal red lines represent a variation of 0%. *n* denotes the number of SWUE for each PFG on which the boxplot has been constructed.

303 five days after nutrient enrichment (Edwards et al., 2005; Hauss et al., 2012; Teixeira et
 304 al., 2018). The reaction durations lasted between two and five days and were positive
 305 for all PFG abundances except for the Orgnano and Orgpicopro cells and for all PFG

306 biomasses except for the Orgpicopro cells. The comparison with previous studies is com-
307 plicated by the different phytoplankton nomenclatures used. For instance, the increase
308 in cyanobacteria abundance shown by Martin-Platero et al. (2018) is difficult to match
309 with either Orgpicopro decreases or Redpicopro increases in abundance. Yet, the joint
310 Redpicopro abundance positive reaction and increase in N/P ratio during the event is
311 consistent with Martiny et al. (2016). Similarly, the co-occurrence of strong biological
312 and N/P variability is in accordance with (Martz et al., 2014). The negative sign of Orgnano
313 reaction could be compared to the curbing abundance of cluster C5 identified in Dugenne
314 et al. (2014) after a wind event. Similarly, Thyssen et al. (2008) have shown that two
315 groups that presented similar red fluorescence/yellow fluorescence profiles as the Org-
316 picopro and Orgnano groups reacted differently than the other functional groups to the
317 SWUEs.

318 After the reaction, the PFGs presented mostly negative relaxation patterns except
319 for Orgpicopro and Orgnano during some SWUEs. As presented in Figure S9 in Sup-
320 plemental Material, there seems to exist an inverse relationship between these two phases
321 for most PFG abundances and biomasses: the more positive the reaction was, the more
322 negative the relaxation will be for a given PFG. This can be interpreted as environmen-
323 tal forces pushing back to the steady state. These forces remain however to be identi-
324 fied and could be of various nature: nutrient depletion (Wilkerson et al., 2006), competi-
325 tion between functional groups (Martin-Platero et al., 2018), viral lysis or predation
326 (Sun et al., 2007; Coello-Camba et al., 2020). Following Hunter-Cevera et al. (2014), the
327 effect of these forces can be estimated using the model loss, i.e. the difference between
328 the observed PFG population growth rates and their estimations by the size-structured
329 model. The authors showed that the more correlated the loss is to the growth rate, the
330 more likely these losses are caused by biological factors. As made visible in Figure S10
331 in Supplemental Information, only the Rednano and Orgnano losses were significantly
332 but weakly correlated ($r \leq 0.31$) with their growth rates in the relaxation phase. These
333 low or non-significant correlations between growth rates and PFG losses seem to indi-
334 cate that physical forces, such as water masses mixing or water column re-stratification,
335 as well as biogeochemical hindrances (e.g. nutrient depletion or co-limitation) are dom-
336 inant during this phase as compared with grazing and viral lysis.

337 The PFG responses have been characterized thanks to a fine temporal and functional-
338 level resolution. As evoked in Martin-Platero et al. (2018), the chosen taxonomic level
339 (taxa, genera, etc.) along with the temporal frequency have a strong impact on the re-
340 sponse patterns observed. In their studies, Martin-Platero et al. (2018) have used Op-
341 erational taxonomic units (OTUs) based on rRNA sequences similarity, while Martiny
342 et al. (2016) relied on functional groups close to the ones of this study obtained using
343 diagnostic pigments. We used automated pulse-shape recording flow cytometry to ob-
344 tain an infra-day resolution over a long period and a resolution up to the cytometric func-
345 tional group. Each functional group contains several ecotypes which could affect the es-
346 timated growth rates (Hunter-Cevera et al., 2014) and add uncertainty to the size-structured
347 model. The effect of complete PFG population replacements that could occur during ex-
348 tremely strong SWUEs may additionally impact the presented estimations. This is also
349 the case of the independence between predator behaviors and the phytoplankton cell sizes
350 assumed by the model that could not be tested here. As a result, the estimated growth
351 rates were principally used to give context to the underlying phenomena and to empha-
352 size the fast and remarkable impacts of SWUE on phytoplankton dynamics. Future re-
353 search could hence use the introduced high-frequency methodology to derive the proper
354 impact of SWUE on phytoplankton primary production.

355 Similarly, while the temporal aspects of such tight biophysical coupled mechanisms
356 are well-resolved by our sampling strategy and numerical approach, the present study
357 did not offer a comprehensive view of the spatial variability at stake. When coupling physics
358 with biology, the observed biological response of the PFGs could dramatically vary de-

359 pending on whether the water masses originated for example from areas near the Deep
 360 Chlorophyll Maximum, the nitracline, or the phosphocline. The phytoplankton biomass
 361 spatial dynamics, approached by chlorophyll-a concentration, have been extensively tracked
 362 by satellite (Wu et al., 2008; d’Ortenzio & Ribera d’Alcalà, 2009; Mayot et al., 2016; Lehahn
 363 et al., 2017; El Hourany et al., 2019). However, the satellites typically have issues resolv-
 364 ing coastal areas and submesoscale patterns, focus on surface waters, have lower tem-
 365 poral resolutions (e.g. daily for sea surface temperature, weekly for clear chlorophyll-a
 366 maps) and hence could not properly resolve the phytoplankton nycthemeral cycles.

367 In this respect, multi-year high-frequency in situ measurements, such as the ones
 368 performed at the SSL@MM coastal laboratory, could bring crucial missing pieces of in-
 369 formation. It could for instance be complementary to the work of Alvain et al. (2008)
 370 that matched chlorophyll-a anomalies resolved by satellite with phytoplankton commu-
 371 nity structures collected in situ. Other methods such as autonomous vehicle fleets (Jaffe
 372 et al., 2017), coastal radars (HFRs) (Cianelli et al., 2017), or 3D models coupling physics
 373 and biogeochemistry (Frayse et al., 2013) could be used jointly with the SSL@MM data
 374 to gain further insights about spatial dynamics and help guide future modeling efforts.

375 In summary, the SWUEs have generated significant abundance and biomass responses
 376 from the pico-nanophytoplankton community. From our data, the biggest daily biomass
 377 increase due to a single wind-induced upwelling represented 97.6% of the daily biomass
 378 increase imputable to the spring bloom. The consistent time scales and magnitudes of
 379 biological responses reported here for sporadic wind-induced events using an innovative
 380 sampling strategy and an advanced statistical methodology could provide new insights
 381 on how to observe, and perhaps model, the impact of other submesoscale events on phy-
 382 toplankton communities.

383 Acknowledgments

384 The authors are grateful to Cytobuoy b.v. for the personalized software developments
 385 performed on the CytoClus4© software features. At the SSL@MM station, the data could
 386 not have been collected without the support of Michel Durand, the MIO Service Atmo-
 387 sphere Mer (Deny Malengros and Fabrice Garcia), and UMS OSU Pytheas (Christian
 388 Marshal and Dorian Guillemain) that maintain the pumping inlet. Additional support
 389 for the SSL@MM was provided by Aix Marseille Université, MIO, and OSU PYTHEAS.
 390 The authors are also very thankful to Ivane Pairaud and the team exploiting the MESURHO
 391 buoy for the PAR data, and to the MIO-PACEM platform for the nutrients analysis. Fund-
 392 ing for R.F.’s Ph.D. thesis was provided by the Ministry of Higher Education, Research,
 393 and Innovation. The project leading to this publication has received funding from the
 394 ERDF under project 1166-39417. The project leading to this publication has received
 395 funding from the Excellence Initiative of Aix-Marseille University - A*MIDEX, a French
 396 “Investissements d’Avenir” program.

397 Open Research

398 The code and data to reproduce the presented results of the paper are available
 399 at <https://github.com/RobeeF/PhytoUpwellingPaper>

400 References

- 401 Alvain, S., Moulin, C., Dandonneau, Y., & Loisel, H. (2008). Seasonal distribu-
 402 tion and succession of dominant phytoplankton groups in the global ocean: A
 403 satellite view. *Global Biogeochemical Cycles*, 22(3).
 404 Antoine, D., Morel, A., & André, J.-M. (1995). Algal pigment distribution and
 405 primary production in the eastern mediterranean as derived from coastal zone
 406 color scanner observations. *Journal of Geophysical Research: Oceans*, 100(C8),

- 16193–16209.
- 407
408 Armbrecht, L. H., Roughan, M., Rossi, V., Schaeffer, A., Davies, P. L., Waite,
409 A. M., & Armand, L. K. (2014). Phytoplankton composition under contrast-
410 ing oceanographic conditions: Upwelling and downwelling (eastern australia).
411 *Continental Shelf Research*, *75*, 54–67.
- 412 Bai, J., & Perron, P. (2003). Critical values for multiple structural change tests. *The*
413 *Econometrics Journal*, *6*(1), 72–78.
- 414 Bakun, A., & Agostini, V. N. (2001). Seasonal patterns of wind-induced up-
415 welling/downwelling in the mediterranean sea. *Scientia Marina*, *65*(3), 243–
416 257.
- 417 Bauer, J. E., Cai, W.-J., Raymond, P. A., Bianchi, T. S., Hopkinson, C. S., & Reg-
418 nier, P. A. (2013). The changing carbon cycle of the coastal ocean. *Nature*,
419 *504*(7478), 61–70.
- 420 Bensoussan, N., Romano, J.-C., Harmelin, J.-G., & Garrabou, J. (2010). High
421 resolution characterization of northwest mediterranean coastal waters thermal
422 regimes: to better understand responses of benthic communities to climate
423 change. *Estuarine, Coastal and Shelf Science*, *87*(3), 431–441.
- 424 Bolaños, L. M., Karp-Boss, L., Choi, C. J., Worden, A. Z., Graff, J. R., Haëntjens,
425 N., ... others (2020). Small phytoplankton dominate western north atlantic
426 biomass. *The ISME journal*, *14*(7), 1663–1674.
- 427 Borges, A. V., Delille, B., & Frankignoulle, M. (2005). Budgeting sinks and sources
428 of co2 in the coastal ocean: Diversity of ecosystems counts. *Geophysical re-*
429 *search letters*, *32*(14).
- 430 Bosc, E., Bricaud, A., & Antoine, D. (2004). Seasonal and interannual variability
431 in algal biomass and primary production in the mediterranean sea, as derived
432 from 4 years of seawifs observations. *Global Biogeochemical Cycles*, *18*(1).
- 433 Brody, S. R., Lozier, M. S., & Dunne, J. P. (2013). A comparison of methods to
434 determine phytoplankton bloom initiation. *Journal of Geophysical Research:*
435 *Oceans*, *118*(5), 2345–2357.
- 436 Cianelli, D., D’Alelio, D., Uttieri, M., Sarno, D., Zingone, A., Zambianchi, E., &
437 d’Alcalà, M. R. (2017). Disentangling physical and biological drivers of phyto-
438 plankton dynamics in a coastal system. *Scientific reports*, *7*(1), 1–15.
- 439 Coello-Camba, A., Diaz-Rua, R., Duarte, C. M., Irigoien, X., Pearman, J. K., Alam,
440 I. S., & Agusti, S. (2020). Picocyanobacteria community and cyanophage
441 infection responses to nutrient enrichment in a mesocosms experiment in
442 oligotrophic waters. *Frontiers in Microbiology*, *11*, 1153. Retrieved from
443 <https://www.frontiersin.org/article/10.3389/fmicb.2020.01153> doi:
444 10.3389/fmicb.2020.01153
- 445 d’Ortenzio, F., & Ribera d’Alcalà, M. (2009). On the trophic regimes of the mediter-
446 ranean sea: a satellite analysis. *Biogeosciences*, *6*(2), 139–148.
- 447 Dubelaar, G. B., & Gerritzen, P. L. (2000). Cytobuoy: a step forward towards using
448 flow cytometry in operational oceanography. *Scientia Marina*, *64*(2), 255–265.
- 449 Dubelaar, G. B., Gerritzen, P. L., Beeker, A. E., Jonker, R. R., & Tangen, K.
450 (1999). Design and first results of cytobuoy: A wireless flow cytometer for
451 in situ analysis of marine and fresh waters. *Cytometry: The Journal of the*
452 *International Society for Analytical Cytology*, *37*(4), 247–254.
- 453 Dugenne, M., Thyssen, M., Nerini, D., Mante, C., Poggiale, J.-C., Garcia, N., ...
454 Grégori, G. J. (2014). Consequence of a sudden wind event on the dynamics of
455 a coastal phytoplankton community: an insight into specific population growth
456 rates using a single cell high frequency approach. *Frontiers in microbiology*, *5*,
457 485.
- 458 Edwards, V., Icely, J., Newton, A., & Webster, R. (2005). The yield of chlorophyll
459 from nitrogen: a comparison between the shallow ria formosa lagoon and the
460 deep oceanic conditions at sagres along the southern coast of portugal. *Estuar-*
461 *ine, Coastal and Shelf Science*, *62*(3), 391–403.

- 462 El Hourany, R., Abboud-abi Saab, M., Faour, G., Mejia, C., Crépon, M., & Thiria,
463 S. (2019). Phytoplankton diversity in the mediterranean sea from satellite data
464 using self-organizing maps. *Journal of Geophysical Research: Oceans*, *124*(8),
465 5827–5843.
- 466 Fraysse, M., Pinazo, C., Faure, V. M., Fuchs, R., Lazzari, P., Raimbault, P., &
467 Pairaud, I. (2013). Development of a 3d coupled physical-biogeochemical
468 model for the marseille coastal area (nw mediterranean sea): what complexity
469 is required in the coastal zone? *PLoS one*, *8*(12), e80012.
- 470 Fuchs, R., Thyssen, M., Creach, V., Dugenne, M., Izard, L., Latimier, M., . . . Pom-
471 meret, D. (2022). Automatic recognition of flow cytometric phytoplankton
472 functional groups using convolutional neural networks. *Limnology and*
473 *Oceanography: Methods*. doi: <https://doi.org/10.1002/lom3.10493>
- 474 García-Reyes, M., Largier, J. L., & Sydeman, W. J. (2014). Synoptic-scale up-
475 welling indices and predictions of phyto-and zooplankton populations. *Progress*
476 *in Oceanography*, *120*, 177–188.
- 477 Gattuso, J., Frankignoulle, M., & Wollast, R. (1998). Carbon and carbonate
478 metabolism in coastal aquatic ecosystems. *Annual Review of Ecology, Evo-*
479 *lution, and Systematics*, *29*, 405–434.
- 480 Grob, C., Ulloa, O., Claustre, H., Huot, Y., Alarcon, G., & Marie, D. (2007). Con-
481 tribution of picoplankton to the total particulate organic carbon concentration
482 in the eastern south pacific. *Biogeosciences*, *4*(5), 837–852.
- 483 Hauss, H., Franz, J. M., & Sommer, U. (2012). Changes in n: P stoichiometry in-
484 fluence taxonomic composition and nutritional quality of phytoplankton in the
485 peruvian upwelling. *Journal of sea Research*, *73*, 74–85.
- 486 Hunter-Cevera, K. R., Neubert, M. G., Olson, R. J., Shalapyonok, A., Solow, A. R.,
487 & Sosik, H. M. (2020). Seasons of syn. *Limnology and oceanography*, *65*(5),
488 1085–1102.
- 489 Hunter-Cevera, K. R., Neubert, M. G., Solow, A. R., Olson, R. J., Shalapyonok, A.,
490 & Sosik, H. M. (2014). Diel size distributions reveal seasonal growth dynamics
491 of a coastal phytoplankton. *Proceedings of the National Academy of Sciences*,
492 *111*(27), 9852–9857.
- 493 Jaffe, J. S., Franks, P. J., Roberts, P. L., Mirza, D., Schurgers, C., Kastner, R., &
494 Boch, A. (2017). A swarm of autonomous miniature underwater robot drifters
495 for exploring submesoscale ocean dynamics. *Nature communications*, *8*(1),
496 1–8.
- 497 Lajaunie-Salla, K., Diaz, F., Wimart-Rousseau, C., Wagener, T., Lefèvre, D., Yohia,
498 C., . . . Pinazo, C. (2021). Implementation and assessment of a carbonate
499 system model (eco3m-carbox v1. 1) in a highly dynamic mediterranean coastal
500 site (bay of marseille, france). *Geoscientific Model Development*, *14*(1), 295–
501 321.
- 502 Lehahn, Y., Koren, I., Sharoni, S., d’Ovidio, F., Vardi, A., & Boss, E. (2017). Dis-
503 persion/dilution enhances phytoplankton blooms in low-nutrient waters. *Nature*
504 *Communications*, *8*(1), 1–8.
- 505 Lévy, M., Ferrari, R., Franks, P. J., Martin, A. P., & Rivière, P. (2012). Bringing
506 physics to life at the submesoscale. *Geophysical Research Letters*, *39*(14).
- 507 Li, W. (1995). Composition of ultraphytoplankton in the central north atlantic. *Ma-*
508 *rine Ecology Progress Series*, *122*, 1–8.
- 509 Lomas, M. W., & Moran, S. B. (2011). Evidence for aggregation and export of
510 cyanobacteria and nano-eukaryotes from the sargasso sea euphotic zone. *Bio-*
511 *geosciences*, *8*(1), 203–216.
- 512 Lomas, M. W., Roberts, N., Lipschultz, F., Krause, J., Nelson, D., & Bates, N.
513 (2009). Biogeochemical responses to late-winter storms in the sargasso sea. iv.
514 rapid succession of major phytoplankton groups. *Deep Sea Research Part I:*
515 *Oceanographic Research Papers*, *56*(6), 892–908.
- 516 Marrec, P., Grégori, G., Doglioli, A. M., Dugenne, M., Della Penna, A., Bhairy,

- 517 N., ... Thyssen, M. (2018). Coupling physics and biogeochemistry thanks
 518 to high-resolution observations of the phytoplankton community structure in
 519 the northwestern mediterranean sea. *Biogeosciences*, *15*(5), 1579–1606. Re-
 520 trieved from <https://bg.copernicus.org/articles/15/1579/2018/> doi:
 521 10.5194/bg-15-1579-2018
- 522 Martin-Platero, A. M., Cleary, B., Kauffman, K., Preheim, S. P., McGillicuddy,
 523 D. J., Alm, E. J., & Polz, M. F. (2018). High resolution time series reveals
 524 cohesive but short-lived communities in coastal plankton. *Nature communica-*
 525 *tions*, *9*(1), 1–11.
- 526 Martiny, A. C., Talarmin, A., Mouginot, C., Lee, J. A., Huang, J. S., Gellene, A. G.,
 527 & Caron, D. A. (2016). Biogeochemical interactions control a temporal suc-
 528 cession in the elemental composition of marine communities. *Limnology and*
 529 *Oceanography*, *61*(2), 531–542.
- 530 Martz, T., Send, U., Ohman, M. D., Takeshita, Y., Bresnahan, P., Kim, H.-J., &
 531 Nam, S. (2014). Dynamic variability of biogeochemical ratios in the southern
 532 california current system. *Geophysical Research Letters*, *41*(7), 2496–2501.
- 533 Mayot, N., d’Ortenzio, F., Ribera d’Alcalà, M., Lavigne, H., & Claustre, H. (2016).
 534 Interannual variability of the mediterranean trophic regimes from ocean color
 535 satellites. *Biogeosciences*, *13*(6), 1901–1917.
- 536 Millot, C. (1979). Wind induced upwellings in the gulf of lions. *Oceanologica Acta*,
 537 *2*(3), 261–274.
- 538 Morel, A., & André, J.-M. (1991). Pigment distribution and primary production
 539 in the western mediterranean as derived and modeled from coastal zone color
 540 scanner observations. *Journal of Geophysical Research: Oceans*, *96*(C7),
 541 12685–12698.
- 542 Odic, R., Bensoussan, N., Pinazo, C., Taupier-Letage, I., & Rossi, V. (2022). Spo-
 543 radic wind-driven upwelling/downwelling and associated cooling/warming
 544 along northwestern mediterranean coastlines. *Continental Shelf Research*
 545 *(under final revision)*.
- 546 Olson, R. J., Shalapyonok, A., & Sosik, H. M. (2003). An automated submersible
 547 flow cytometer for analyzing pico-and nanophytoplankton: Flowcytobot. *Deep*
 548 *Sea Research Part I: Oceanographic Research Papers*, *50*(2), 301–315.
- 549 Pairaud, I., Gatti, J., Bensoussan, N., Verney, R., & Garreau, P. (2011). Hydrology
 550 and circulation in a coastal area off marseille: Validation of a nested 3d model
 551 with observations. *Journal of marine systems*, *88*(1), 20–33.
- 552 Palma, E. D., & Matano, R. P. (2009). Disentangling the upwelling mechanisms of
 553 the south brazil bight. *Continental Shelf Research*, *29*(11-12), 1525–1534.
- 554 Ribalet, F., Swalwell, J., Clayton, S., Jiménez, V., Sudek, S., Lin, Y., ... Armbrust,
 555 E. V. (2015). Light-driven synchrony of prochlorococcus growth and mor-
 556 tality in the subtropical pacific gyre. *Proceedings of the National Academy of*
 557 *Sciences*, *112*(26), 8008–8012.
- 558 Richardson, T. L., & Jackson, G. A. (2007). Small phytoplankton and carbon export
 559 from the surface ocean. *Science*, *315*(5813), 838–840.
- 560 Rossi, V., Garçon, V., Tassel, J., Romagnan, J.-B., Stemmann, L., Jourdin, F., ...
 561 Morel, Y. (2013). Cross-shelf variability in the iberian peninsula upwelling sys-
 562 tem: Impact of a mesoscale filament. *Continental Shelf Research*, *59*, 97–114.
- 563 Rossi, V., Schaeffer, A., Wood, J., Galibert, G., Morris, B., Sudre, J., ... Waite,
 564 A. M. (2014). Seasonality of sporadic physical processes driving tempera-
 565 ture and nutrient high-frequency variability in the coastal ocean off southeast
 566 australia. *Journal of Geophysical Research: Oceans*, *119*(1), 445–460.
- 567 Sapiano, M., Brown, C., Schollaert Uz, S., & Vargas, M. (2012). Establishing a
 568 global climatology of marine phytoplankton phenological characteristics. *Jour-*
 569 *nal of Geophysical Research: Oceans*, *117*(C8).
- 570 Sosik, H. M., Olson, R. J., Neubert, M. G., Shalapyonok, A., & Solow, A. R. (2003).
 571 Growth rates of coastal phytoplankton from time-series measurements with a

- 572 submersible flow cytometer. *Limnology and Oceanography*, 48(5), 1756–1765.
- 573 Sun, J., Feng, Y., Zhang, Y., & Hutchins, D. (2007, 09). Fast microzooplankton
574 grazing on fast-growing, low-biomass phytoplankton: A case study in spring in
575 chesapeake bay, delaware inland bays and delaware bay. *Hydrobiologia*, 589,
576 127–139. doi: 10.1007/s10750-007-0730-6
- 577 Teixeira, I., Arbones, B., Froján, M., Nieto-Cid, M., Álvarez-Salgado, X. A., Cas-
578 tro, C. G., ... Figueiras, F. (2018). Response of phytoplankton to enhanced
579 atmospheric and riverine nutrient inputs in a coastal upwelling embayment.
580 *Estuarine, Coastal and Shelf Science*, 210, 132–141.
- 581 Thyssen, M., Fuchs, R., Créach, V., Artigas, L. F., Grégori, G., Marrec, P., ... oth-
582 ers (2021). Standard vocabulary, consensual functional groups and automated
583 classification for phytoplankton high throughput datasets using automated flow
584 cytometry. In *Aslo 2021*.
- 585 Thyssen, M., Mathieu, D., Garcia, N., & Denis, M. (2008). Short-term variation of
586 phytoplankton assemblages in mediterranean coastal waters recorded with an
587 automated submerged flow cytometer. *Journal of Plankton Research*, 30(9),
588 1027–1040.
- 589 Tréguer, P., & Le Corre, P. (1975). Manuel d’analyse des sels nutritifs dans l’eau de
590 mer (utilisation de l’autoanalyseur ii technicon), 110, lab. d’océanogr. *Chim.,*
591 *Univ. de Bretagne Occident., Brest, France*.
- 592 Truong, C., Oudre, L., & Vayatis, N. (2020). Selective review of offline change point
593 detection methods. *Signal Processing*, 167, 107299.
- 594 Wilkerson, F. P., Lassiter, A. M., Dugdale, R. C., Marchi, A., & Hogue, V. E.
595 (2006). The phytoplankton bloom response to wind events and upwelled
596 nutrients during the coop west study. *Deep Sea Research Part II: Topical*
597 *Studies in Oceanography*, 53(25-26), 3023–3048.
- 598 Wimart-Rousseau, C., Lajaunie-Salla, K., Marrec, P., Wagener, T., Raimbault, P.,
599 Lagadec, V., ... others (2020). Temporal variability of the carbonate system
600 and air-sea co2 exchanges in a mediterranean human-impacted coastal site.
601 *Estuarine, Coastal and Shelf Science*, 236, 106641.
- 602 Wu, Y., Platt, T., Tang, C. C., Sathyendranath, S., Devred, E., & Gu, S. (2008). A
603 summer phytoplankton bloom triggered by high wind events in the labrador
604 sea, july 2006. *Geophysical Research Letters*, 35(10).